J. Sci. Trans. Environ. Technov. 2023, 17 (2) : 36 - 44

An Innovative Analysis of Multi-Modal Co-Learning on PET-CT Images for Liver Lesion Segmentation

T. Haripriya and K. Dharmarajan

[1] Research Scholar, School of computing Sciences, VISTAS, Chennai, India. email : hariswt9@gmail.com
[2] Associate Professor, School of computing Sciences, VISTAS, Chennai, India. email : dharmak07@gmail.com

Article History
Received: **10.10.2023**
Revised and Accepted: **13.11.2023**
Published: **16.12.2023**

https://doi.org/10.56343/STET.116.017.002.006
www.stetjournals.com

ABSTRACT

Positron emission tomography and computed tomography (PET-CT) imaging is a tool extensively used for detecting liver lesions (FLLs). Still, distinguishing these contemporary styles will ignore some of the information astride the two processes while features interact, count the collaborative literacy of the point chart of various judgments, and not make sure that shallow and deep aspects regard each other adequately. In this paper, our proposed model can attain feature relations along the multi-modal channels by sharing each down sampling block among two encoding branches to remove deceiving features. Also, we integrate feature maps of various plans to derive spatially varying fusion maps and elaborate the lesion's information. In addition, we initiate a resemblance loss function for thickness constraints in the event that the forecasts of separated refactoring branches for the same field differ a lot. We estimate our model for liver excrescence segmentation using a PET-CT scan dataset, compare our system with the baseline approach for multi- modal (multi-branches, multi-channels, and cascaded networks), and also justify that our system has a fully advanced delicacy ($p < 0.06$) than the base line models.

Keywords: convolutional neural networks, liver lesion segmentation, Ultrasound, multi-modal collaborative literacy, PET- CT

1. INTRODUCTION

One of the fatal and utmost dangerous conditions in the world is liver complaint. Around 2.8 of deaths in India occur as a result of liver complaint each time. Due to its unpretentious symptoms, liver complaint can be grueling to diagnose in its early stages. Constantly, the symptoms can show up only when it's too late. Liver lesion segmentation plays a very important role in computer aided prognosis and treatments. It also helps to identify other disease by image guided surgery and the visualization of medical data for clinical diagnosis and pathogeny research. The high likeness in intensities between the liver tissue and the adjacent organs, the diversity in the liver shape, and the random manifestations of lesions, furthermore it is a challenging task to segment the normal from the infected regions from CT images. Image-based automatic segmentation of liver tumors can help surgeon to accurately locate the tumors, their sizes and visualize the relationship among the cancer lesions and the enclosing blood vessels and liver tissue. While, we using manual segmentation the clinical application is time consuming. In a multiplicity of medical imaging techniques, computed tomography (CT) images are frequently used in computer-aided prognostic and surgical planning due to their high signal-to-noise ratio and better spatial plan. In spite of the CT only reflects the structures of organs without providing any practical details. Cancer cells are generally more metabolically active, and various kind of tumors have

T. Haripriya
Research Scholar, School of computing Sciences, VISTAS, Chennai, India
email : hariswt9@gmail.com

P-ISSN 0973-9157
E-ISSN 2393-9249

a preference for glucose in terms of energy sources, which is the reason that 18F flurodeoxyglucose (18F-FDG) PET can be used for tumor visualization. PET is an imaging technology that shows the bio molecular metabolism, receptor and neuromedia activity in living organisms, with a high sensitivity and a high specificity, and can therefore be used to assist in diagnosis.

Hepatocellular carcinoma (HCC) has various shapes, sizes, locations and pathological properties for each patient. Infig.1, however lesion as shown in first two columns, sometimes we can locate only mutilated lesions on CT or PET imaging as shown in the remaining columns. In these cases, when the lesions and the bounding tissues have a similar anatomical structure on CT images, PET can distinguish them for their different metabolic intensities; meanwhile, CT can locate the necrotic regions which show a low metabolism on the PET images. Therefore combining PET and CT scans not only provides more information about lesions and their adjacent tissues, but it also can make imaging features complement each others. In contrast, multi-modal medical scans have been used for organ lesions segmentation and detection by deep CNN and handcrafted features.

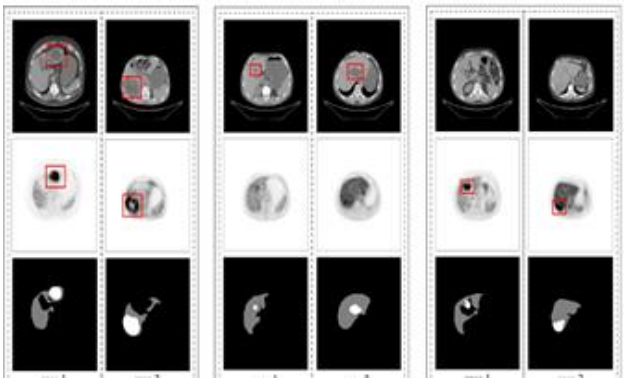

Figure 1 (a) Obvious lesions (b) Obvious lesions (c) Obvious

Figure 1: PET scans are unified to the same resolution as CT through interpolation, then CT and PET images are processed by affine alignment. The original CT images (the first row), their corresponding PET images (the second row) and the ground truth of liver and liver lesions (the third row). (A) An example of obvious lesion regions on both PET and CT images, (B) Shows tumors that are obviously reflected on CT images but hidden in the PET images, and (C) illustrates cases where lesions are obviously distinguished on PET images but hardly on CT images. Therefore, multi-modal PET-CT scans can complement each others to obtain a better liver lesion segmentation performance.

They put out a technique for fuzzy Markov random field modelling to automatically segment lung tumors on PET-CT data. They applied random walks to PET and CT imaging, respectively, and summarised two weighted probability maps to get the final prediction findings. U-Net and V-Net are the two most widely used networks for medical image segmentation tasks because of their straightforward but efficient CNN designs. In addition, many other successful variant networks built on UNet exist. Blocks are crucial for the final segmentation outcome and are taken from all encoders; therefore a network structure that employs feature information is used. They presented a deep learning method for tumor segmentation on PET-CT images of patients with head and neck malignancies. We contend that each intermediate PET block can effectively give pathological information, and the CT block should provide anatomical information during feature extraction, taking into consideration the structural and spatial consistency between two blocks at the same level. Therefore, we suggest a brand-new Shared Down-sampling Block (SDB) that the CT and PET encoder blocks at the U-Net and V- Net are the two most widely used networks for medical image segmentation tasks because of their straight forward but efficient CNN designs. In addition, many other successful variant networks built on U Net exist. Blocks are crucial for the final segmentation outcome and are taken from all encoders; therefore a network structure that employs feature information is used. Recently, only a few methods have been proposed for liver lesions segmentation on multi-modal PET-CT scans. Existing multi-modal co-learning methods can mainly be summarized as follows: feature extraction from each modality, followed by a combination of modality-specific features with CNN architecture or traditional methods. For the generation of the probability maps from the different modalities, current deep learning methods have separate encoder architecture for each modality. Traditional methods apply wavelet-based and transform-based theory for

feature decomposition, local energy, and weighted regional variance for feature extraction and feature fusion. However, there is a common drawback with the existing multi-modal feature extraction methods. The CT encoder blocks benefit only from the upper levels that generate CT probability maps. On the other hand, the PET encoders at the upper layer do not contribute to anything. Considering the structural and spatial consistency between two blocks at the same level, we argue that each intermediate PET block can provide effective pathological information, and the CT block should provide anatomical information during feature extraction. Hence, we propose a novel shared down sampling block (SDB) that can be used by the CT and PET encoder blocks at the same depth within the network.

The authors propose three new feature co-learning methods for PET-CT image segmentation. The first involves a single feature decoder (SDB) that extracts pathological information from PET-CT data, while the second involves combining fusion features volumes in HFCM. Hierarchical skip connections transmit more features information from FCBs to the decoder branch, prioritizing lesions features. Two image refactoring branches are designed, one without HFCM and the other focusing on hidden lesions in fusion feature maps. The decoder branches segment the lesions in the same PET-CT volumes, and a similarity loss is proposed to penalize discrepancies between predictions.

II. MATERIALS

A. Datasets

In our research, we make use of the 100 FDG PET-CT scans that were split into 10 subsets for 10-fold cross validation.The liver contour and lesion masks have been labelled by skilled radiologists using a dataset that has been provided by Shanghai BNC.

In this dataset, there are between 1 and 30 thorax-regional tumors per case and there are between 5 and 109 slices of liver lesions. A 3D tumor's volume can range from 624 cm3 to 939053 cm3, and the maximum cross-sectional area of liver tumors is between 129 cm2 and 14026 cm2. Because of the wide range of tumor volume and its variations, it can be inferred from the analysis of the materials above that automatic liver lesion segmentation is a difficult task.

B. Data Preprocessing

In our experiment, we pre-process the PETCT images before supplying them to our network in an effort to improve performance and hasten convergence. Since the PET pixel values range from 0 to several hundred thousands, they are more difficult to normalize than CT data, according to study of the raw data. Standard Uptake Value (SUV) conversion is done for PET pixel data. The PET-CT data must first be resample to be consistent at 256*256 pixels (x-y axis) before being subjected to co-learning. To combine the characteristics of the multi-modal images for registration, the thickness of the PET and CT scans must also be unified. We also use an affine alignment to prevent the PET-CT images from shifting. Physicians commonly use affine registration for PET-CT tumor volume delineation, with affine transformation for simplicity. In this research, liver lesions locations on PET and CT images are consistent.

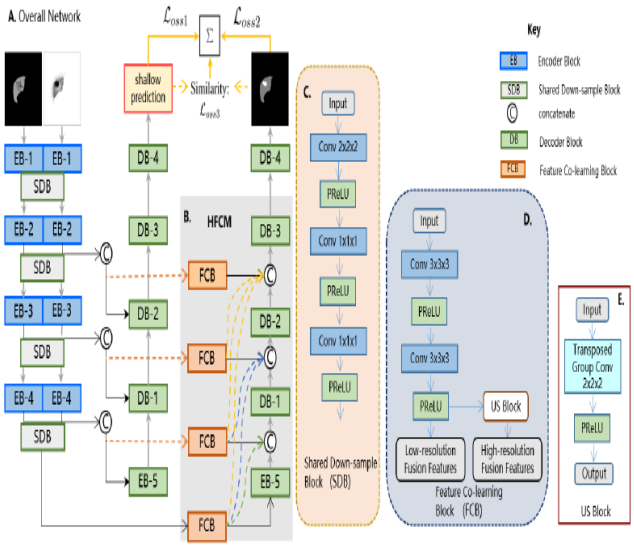

Figure. 2: Overall Architecture

Figure. 2: The proposed network methods have an overall architecture consisting of SDB (shared down-sampling block), FCB (feature co learning block), and US (up-sampling block). The first layer enters DB-1, followed by DB-2 and DB-3, with skip connections from FCB to the right decoder branch.

The proposed Hierarchical Feature Co-Learning Module (HFCM) consists of four FCBs with hierarchical skip connections. The left decoder branch is marked as T1, and the right one as T2.

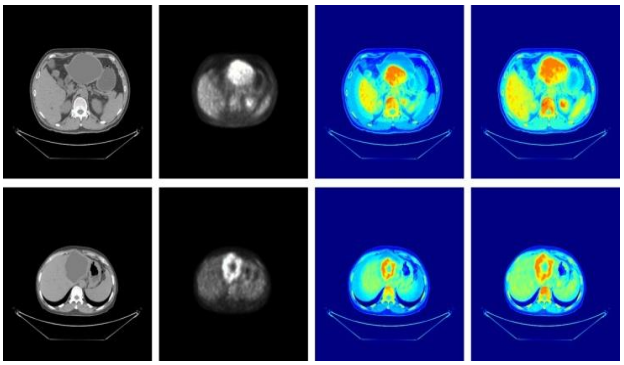

CT **PET** **before** **after**

Figure 3: Visual comparison of the results obtained by affine alignment compared to the original PET-CT fusion image. The first two columns show original CT images and PET images, the following two columns show the fusion results of original PET-CT pairs and results after affine alignment.

III. METHODS

This paper uses V-Net and morphological processing to extract liver contours from masked PET-CT images, forming a fusion co-learning network with two main parts. They are SDB and HFCM.

A. Liver Contour

V-Net model extracts liver contour from CT scans, combined with PET data for liver lesion segmentation.The CT regions outside the liver contour to -200, and set the values of the same positions on the PET images to 0.01. Therefore, the liver masks can avert the impact of Irrelevant organs and tissues.

B. Shared Down sampling block

Multi-modal data is often extracted using multiple encoder branches for segmentation or detection tasks. This approach does not benefit PET and CT scans, but it ensures consistent lesions at the same locations. Unique labels are used in the learning process, and CT images can be attenuated and corrected if the PET image's anatomical structure is clear. CT images can be attenuated

C. Hierarchical feature co-learning module

Deep CNN features extraction varies between shallow and deep layers, with shallow structures capturing simple features like edges and boundaries, while deep layers capture higher-level features due to their broader receptive field and more convolution operations. To fuse lesions information at different depths, HFCM is proposed. The hierarchical feature co-learning module consists of two components: the feature co-learning block combining anatomical and functional features from PET and CT, and the up-sampling block resizing fusion feature volumes to derive spatially varying fusion maps. The feature volumes are fed to decoders at different levels. Hierarchical skip connections generate more information exchange between the FCB and decoder blocks, resulting in liver lesion features being prioritized during image reconstruction.

D. Loss function

Medical image segmentation often faces imbalances in category labels, leading to various loss functions designed to address this issue. Focal loss aims to address the imbalance between background and foreground in object detection, while dice loss compares prediction results with labels. Tversky loss is a sum of weighted dice loss and focal loss, with the weight determining precision or sensitivity. This paper adopts dice loss for liver contour segmentation and Focal Tversky loss function for liver lesions segmentation.

IV. EXPERIMENTS

The study validates liver contours and lesions segmentation experiments on 100 PET-CT scans using pre-processing and hyper-parameters. Repeated tests and ANOVAs are performed on each model, revealing statistically significant differences between models. The experimental settings and parameters are presented, and the SDB module is tested. The HFCM method is adopted, and the method is compared with existing methods to prove its effectiveness.

A. Training and Testing

The proposed method for liver lesions segmentation consists of two stages: stage-1, which deals with liver contour segmentation, and stage-2, which covers liver lesion segmentation. Masked

PET-CT scans are used for all contrastive methods. The liver contour segmentation process involves resampling the CT series to a uniform resolution, retaining blocks containing the liver organ, and truncating block values to the range of -200 to 400 HU. The data is fed into V-Net for liver contour segmentation training, and the model converges after 80 epochs. Morphological post-processing is performed after the deep network prediction to improve results. The liver is a connected organ in the human body, but the prediction map may have isolated areas. The segmentation edges are optimized using expansion corrosion, and the largest connectivity domain in 3-dimensional space is chosen as the liver profile. Morphological post-processing methods improve the dice score of liver contour segmentation by 1.05% (95:65% vs. 96:70%).

The proposed network focuses on accelerating network convergence and ignoring irrelevant information to focus on lesions. The network is implemented using the Pytorch library and employs gradient descent optimization algorithms. The training process is performed on a PC with a NVIDIA Tesla V100 GPU, taking 12 hours for 300 epochs. The prediction result is the sum of outputs generated by the two branches, with their weights set to be the same as the weights used in the training phase.

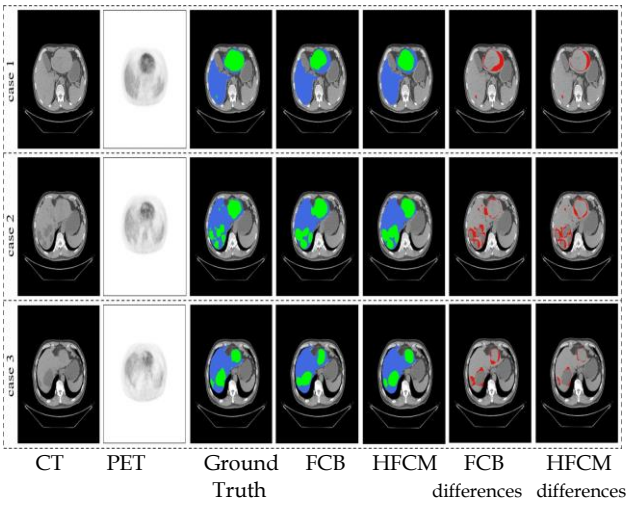

Figure 4: Comparison of FCB and HFCM segmentation results based on three cases. The first three columns are CT, PET andthe ground truth images, the following two columns show the prediction results of the models with FCB and HFCM, and the last two columns present the difference between the prediction results and the ground truth. Blue, green and red delineations mean normal liver regions, liver lesions and where lesions were incorrectly segmented, respectively.

TABLE 1: Comparison of baseline models with and without SDB. The segmentation performance is measured with the dice score (%), **[Mean Standard Deviation]** and hausdorff distance (*mm*). In the results of repeated statistical analysis, if the value of PR is lower than 0.05, the difference is statistically significant.

Metrics of experimental scores

Model	**Dice per case (%)**	**Dice global (%)**	**Hausdorff Distance (mm)**
2D U-Net two-encoder	57.73 ± 1.07	60.00 ± 1.49	68.2014
2D U-Net two-encoder +SDB	59.02 ± 0.92	61.57 ± 1.13	64.3729
3D V-Net two-encoder	64.38 ± 1.01	64.35 ± 2.07	60.0249
3D V-Net two-encoder + SDB	65.67 ± 0.84	66.65 ± 1.25	57.6326

Metrics of experimental scores

Model	Dice per case (%)	Dice global (%)	Hausdorff Distance (mm)
2D U-Net two-encoder	58.75 ± 1.08	65.00 ± 1.50	69.2015
2D U-Net two-encoder +FCB	62.84 ± 1.05	63.79 ± 0.75	59.2646
2D U-Net two-encoder + HFCM	**64.75 ± 0.95**	**65.17 ± 1.08**	54.6039
3D V-Net two-encoder	65.39 ± 1.02	65.36 ± 3.08	61.0349
3D V-Net two-encoder + FCB	66.82 ± 1.07	68.42 ± 1.12	58.2935
3D V-Net two-encoder + HFCM	**69.15 ± 0.95**	**69.78 ± 1.02**	58.7079

TABLE II: Effect of FCB and HFCM based on baseline models. HFCM consists of several FCBs with hierarchical skip connections. The performance is measured with dice per case score (%), **[Mean Standard Deviation]** and hausdorff distance (*mm*). In the results of repeated statistical analysis, if the value of PR is lower than 0.05, the difference is statistically significant.

B. Ablation study

PET and CT scans offer distinct advantages for pathological analysis, such as detecting necrotic liver regions due to low metabolism and similar density to infected liver issues in CT scans. PET scans have better spatial resolution on lesions, particularly malignant tumor tissues, while CT images accurately reflect organ tissue anatomy, locate lesions, and show morphology. Traditional multi-modal feature fusion networks have two encoders, but PET and CT branches do not benefit from each other in feature extraction. A more efficient approach is proposed, which uses convolution kernels to process PET and CT data simultaneously. To improve information transmission between FCB and decoder branch encoders extract feature volumes at different depths within the network. The feature fusion module then feeds these volumes to each feature co-learning block, allowing them to absorb multi-modal information at different resolutions.

TABLE III: Results of 10-fold cross validation for hyper parameters in loss function. The performance is measured with dice per case score (%), **[Mean ± Standard Deviation]**

λ_1	λ_2	μ	Dice per case (%)
0.8	0.4	0.5	69.26 ± 0.75
0.4	0.8	0.5	70.15 ± 0.56
0.6	0.5	0.5	70.95 ± 0.77
0.6	0.5	0.5	71.17 ± 0.58
0.5	**0.5**	**0.5**	**75.73 ± 0.52**

TABLE IV: Different multi-modal fusion methods on 100 PET-CT dataset. The performance is measured with dice per case score and dice global score (%), [Mean _ Standard Deviation], and results of repeated measures statistical analysis of variance between different multi-modal co-learning models. If the value of PR is lower than 0.05, difference is statistically significant.

Metrics of experimental scores

Model	Dice per case (%)	Dice global (%)	Hausdorff Distance (mm)
2D U-Net two-encoder (Baseline)	58.75 ± 1.08	65.00 ± 1.50	69.2015
2D U-Net two-channel	62.84 ± 1.05	63.79 ± 0.75	59.2646
3D V-Net two-encoder (Baseline)	**64.75 ± 0.95**	**65.17 ± 1.08**	54.6039
3D V-Net two-channel	65.39 ± 1.02	65.36 ± 3.08	61.0349
Cascaded U-Net	55.05 ± 0.99	65.73 ± 1.52	59.2454
Cascaded V-Net	67.48 ± 1.08	68.25 ± 0.68	67.4574
2D U-Net two-encoder + SDB + HFCM	66.82 ± 1.07	68.42 ± 1.12	58.2935
3D V-Net two-encoder + SDB + HFCM	68.98 ± 0.65	70.29 ± 0.97	56.1376
Zhao et al.	67.24 ± 0.73	68.13 ± 0.87	68.1447
Zhong et al.	68.85 ± 0.97	69.84 ± 1.02	57.4419
Kumar et al.	69.07 ± 0.48	70.03 ± 1.28	65.2335
ours	**70.71 ± 0.57**	**71.40 ± 0.45**	**48.0264**

C. Comparison with previous works

Our method compared with previous medical segmentation models using the same dataset, applying pre-processing and post processing steps. PET and CT data were fed into two branches for two-encoder models.The proposed model, combining CT scans across channels and output from the first component, outperforms state-of-the-art deep neural networks and co-learning methods. It achieves a significant improvement in dice score with the same hyper-parameter settings, with a PR value of less than 0.05 indicating statistical significance.

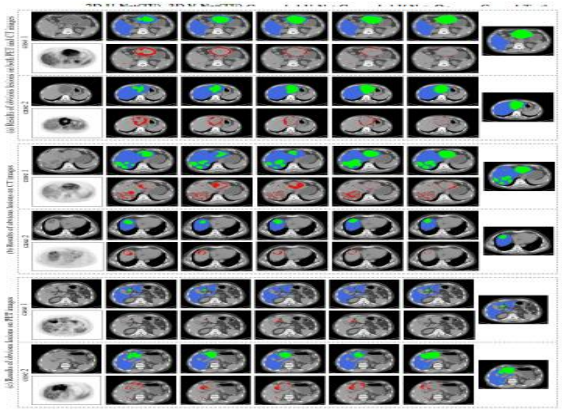

Fig 5: Results of lesions that is obvious on both PET and CT images, only on CT images and only on PET images respectively. In each case, the first column corresponds to the original CT and PET images, the following five figures of the first row show the prediction results of the five different networks (two models with two encoder branches called TE, two Cascaded networks and our method), and the red delineations in the five remaining images of the second row show where the liver lesions were incorrectly segmented. The last column is the corresponding ground truth for these cases.

V. DISCUSSION

The experimental results show that our method outperforms previous techniques in locating large lesion regions (Kitao *et al*., 2009, Piscaglia *et al*., 2010, Goceri *et al*., 2016, Kono *et al*., 2017, Omata *et al*., 2017, Heimbach *et al*.,2018, Morgan *et al*., 2018, Wan *et al.*, 2020, Lee *et al*., 2021, Xue *et al*., 2021, Zhou *et al*.,2021, Turco *et al*., 2022, Sridhar *et al*., 2023). The first group of lesions features is evident on PET and CT images, and all five models can accurately locate the largest lesion region. The SDB module complements feature information from PET and CT scans, resulting in less false positive and negative delineation. The method also performs well when liver lesions vary greatly, with feature maps of small resolution having wider receptive fields and better understanding of tumor edges. The fusion co-learning module in HFCM can use most features from different levels multiple times, providing abstract features and detailed edge information. In the first case of the third group, both cascaded methods miss small lesions, but our model can locate isolated and small lesions more precisely.

The proposed model for liver lesion segmentation uses deep layers and features to improve performance. However, the model's size and fine morphological post processing require liver contour segmentation, which may not be conducive to its extensibility. The evaluation experiments are conducted on PET-CT scans, but other organs or modality scans may have different functional and structural information. The method has flaws in segmenting small lesions, such as the first and last groups, which could be caused by information loss due to image data resampling. Multimodal data alignment is necessary before feeding into deep learning models for better performance. To avoid registration deviations, concatenations between PET-CT encoder branches and FCB modules are only used. Furthermore should address these issues to improve the model's performance.

CONCLUSION

We suggest a computer-aided diagnosis system that combines a hand-crafted and deep feature too effectively difference atypical hepatocellular carcinoma and focal nodular hyperplasia. In this study, Hepatocellular melanoma is a common nasty excrescence with a low early opinion rate. PET-CT scans enhance clarity, particularity, and discovery capacity of micro-lesions. Our approach is executed in the PyTorch. Proposed a multi-modal co-learning network enhances image quality by detecting salient features during the emulsion process, enabling timely lesions identification. As a result, our algorithm holds significant potentiality for clinical usages in abnormal HCC diagnosis, the lesions on other organs or other modality scans may have other functional and structural information, which needs different hyperactive parameters and branches. We aim to address this in our future investigation.

REFERENCE

Goceri, E, Shah, Z.K, Layman, R, Jiang, X, and Gurcan, M.N. 2016. Quantification of liver fat: A comprehensive review. *Comput. Biol. Med*. 71: 174–189. https://doi.org/10.1016/j.compbiomed.2016.02.013 PMid:26945465

Heimbach JK, Kulik LM, Finn RS, Sirlin CB, Abecassis MM, Roberts LR, Zhu AX, Murad MH, and Marrero JA. 2018. AASLD guidelines for the treatment of hepatocellular carcinoma. Hepatology. 2018 Jan;67(1):358-380. doi: 10.1002/hep.29086. https://doi.org/10.1002/hep.29086 PMid:28130846

Kitao A, Zen Y, Matsui O, Gabata T, and Nakanuma Y.2009. Hepatocarcinogenesis: multistep changes of drainage vessels at CT during arterial portography and hepatic arteriography--radiologic-pathologic correlation. *Radiology*. 252(2):605-14. https://doi.org/10.1148/radiol.2522081414 PMid:19703890

Kono Y, Lyshchik A, Cosgrove D, Dietrich CF, Jang HJ, Kim TK, Piscaglia F, Willmann JK, Wilson SR, Santillan C, Kambadakone A, Mitchell D, Vezeridis A, and Sirlin CB.2017. Contrast Enhanced Ultrasound (CEUS) Liver Imaging Reporting and Data System (LI-RADS®): the official version by the American College of Radiology (ACR). Ultraschall Med. 38(1):85-86. https://doi.org/10.1055/s-0042-124369 PMid:28249328

Lee SG, Kim E, Bae JS, Kim JH, and Yoon S.2021. Robust end-to-end focal liver lesion detection using unregistered multiphase computed tomography images. *IEEE Transactions on Emerging Topics in Computational Intelligence*. 2021 Dec. pp.1-15.

Morgan T.A., Maturen K.E., Dahiya N., Sun M.R.M., and Kamaya A.2018. American College of Radiology Ultrasound Liver Imaging and Reporting Data System (US LI-RADS) Working Group. US LI-RADS: Ultrasound liver imaging reporting and data system for screening and surveillance of hepatocellular carcinoma. *Abdom. Radiol.* 43:41–55. https://doi.org/10.1007/s00261-017-1317-y PMid:28936543

Omata M, Cheng AL, Kokudo N, Kudo M, Lee JM, Jia J, Tateishi R, Han KH, Chawla YK, Shiina S, Jafri W, Payawal DA, Ohki T, Ogasawara S, Chen PJ, Lesmana CRA, Lesmana LA, Gani RA, Obi S, Dokmeci AK, and Sarin SK. 2017.Asia-Pacific clinical practice guidelines on the management of hepatocellular carcinoma: a 2017 update. *Hepatol Int.* 2017 Jul;11(4):317-370. https://doi.org/10.1007/s12072-017-9799-9 PMid:28620797 PMCid:PMC5491694

Piscaglia, Fabio , Lencioni, Riccardo , Sagrini, Elisabetta , Pina, Clotilde , Cioni, Dania , Vidili, Gianpaolo and Bolondi, Luigi. 2010. Characterization of Focal Liver Lesions with Contrast-Enhanced Ultrasound. *Ultrasound in medicine & biology*. 36. 531-50. 10.1016/j.ultrasmedbio.2010.01.004.. https://doi.org/10.1016/j.ultrasmedbio.2010.01.004 PMid:20350680

Professional Committee for Prevention and Control of Hepatobiliary and Pancreatic Diseases of Chinese Preventive Medicine Association;; Professional Committee for Hepatology, Chinese Research Hospital Association;; Chinese Society of Hepatology, Chinese Medical Association;; Prevention of Infection Related Cancer (PIRCA) Group, Specialist Committee of Cancer Prevention and Control of Chinese Preventive Medicine Association. [Guideline for stratified screening and surveillance of primary

liver cancer(2020 Edition)]. *Zhonghua Gan Zang Bing Za Zhi*. 2021 Jan 20;29(1):25-40. Chinese. doi: 10.3760/cma.j.cn112152-20201109-00970. PMID: 33541021

Sridhar,J., K.Rajitha, K.Prathyusha, P.Punith Varma, and V.Revanth. 2023. Prediction of liver chronic disease for health care services. International *Journal of Creative Research Thoughts (IJCRT*) 11(3): i101-106.

Turco S, Tiyarattanachai T, Ebrahimkheil K, Eisenbrey J, Kamaya A, Mischi M, Lyshchik A, and El Kaffas A.2022. Interpretable machine learning for characterization of focal liver lesions by contrast-enhanced ultrasound. *IEEE Transactions on ultrasonics, ferroelectrics, and frequency control*.69(5):1670-81 https://doi.org/10.1109/TUFFC.2022.3161719
PMid:35320099 PMCid:PMC9188683

Wan P, Chen F, Shao W, Liu C, Zhang Y, Wen B, Kong W, and Zhang D.2020. Irregular respiratory motion compensation for liver contrast-enhanced ultrasound via transport-based motion estimation. *IEEE Transactions on Ultrasonics, Ferroelectrics, and Frequency Control*.68(4):1117-30. https://doi.org/10.1109/TUFFC.2020.3033984
PMid:33108284

Xue Z, Li P, Zhang L, Lu X, Zhu G, Shen P, Shah SA, and Bennamoun M.2021. Multi-modal co-learning for liver lesion segmentation on PET-CT images. *IEEE Transactions on Medical Imaging*.40(12):3531-42 https://doi.org/10.1109/TMI.2021.3089702
PMid:34133275

Zhou J, Pan F, Li W, Hu H, Wang W,and Huang Q.2021. Feature fusion for diagnosis of atypical hepatocellular carcinoma in contrast-enhanced ultrasound. *IEEE Transactions on Ultrasonics, Ferroelectrics, and Frequency Control.* 69(1):114-23. https://doi.org/10.1109/TUFFC.2021.3110590
PMid:34487493